

A Novel NAMPT Inhibitor-Based Antibody–Drug Conjugate Payload Class for Cancer Therapy

Niels Böhnke,* Markus Berger, Nils Griebenow, Antje Rottmann, Michael Erkelenz, Stefanie Hammer, Sandra Berndt, Judith Günther, Antje M. Wengner, Beatrix Stelte-Ludwig, Christoph Mahler, Simone Greven, Lisa Dietz, Hannah Jörißen, Naomi Barak, Ulf Bömer, Roman C. Hillig, Uwe Eberspacher, Jörg Weiske, Anja Giese, Dominik Mumberg, Carl Friedrich Nising, Hilmar Weinmann, and Anette Sommer

Cite This: *Bioconjugate Chem.* 2022, 33, 1210–1221

Read Online

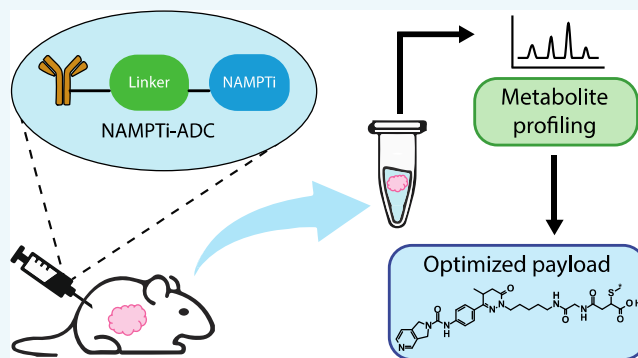
ACCESS |

Metrics & More

Article Recommendations

Supporting Information

ABSTRACT: Inhibition of intracellular nicotinamide phosphoribosyltransferase (NAMPT) represents a new mode of action for cancer-targeting antibody–drug conjugates (ADCs) with activity also in slowly proliferating cells. To extend the repertoire of available effector chemistries, we have developed a novel structural class of NAMPT inhibitors as ADC payloads. A structure–activity relationship-driven approach supported by protein structural information was pursued to identify a suitable attachment point for the linker to connect the NAMPT inhibitor with the antibody. Optimization of scaffolds and linker structures led to highly potent effector chemistries which were conjugated to antibodies targeting C4.4a (LYPD3), HER2 (c-erbB2), or B7H3 (CD276) and tested on antigen-positive and -negative cancer cell lines. Pharmacokinetic studies, including metabolite profiling, were performed to optimize the stability and selectivity of the ADCs and to evaluate potential bystander effects. Optimized NAMPTi-ADCs demonstrated potent *in vivo* antitumor efficacy in target antigen-expressing xenograft mouse models. This led to the development of highly potent NAMPT inhibitor ADCs with a very good selectivity profile compared with the corresponding isotype control ADCs. Moreover, we demonstrate—to our knowledge for the first time—the generation of NAMPTi payload metabolites from the NAMPTi-ADCs *in vitro* and *in vivo*. In conclusion, NAMPTi-ADCs represent an attractive new payload class designed for use in ADCs for the treatment of solid and hematological cancers.



INTRODUCTION

With the approval of so far 12 antibody–drug conjugates (ADCs) and more than 100 ADCs in clinical trials,^{1–5} the landscape of ADCs has evolved rapidly during the last decade. Most ADCs employ payloads acting on cell proliferation, including microtubule-destabilizing drugs such as auristatins and maytansinoids, or DNA-targeted drugs such as calicheamicins, topoisomerase inhibitors, and pyrrolobenzodiazepines.⁶ Thus, we sought to identify payloads with an alternative mode of action that may allow the targeting of tumors with a lower proliferation rate to complement the available set of payload classes.

Nicotinamide adenine dinucleotide (NAD⁺) is an essential coenzyme in redox reactions and, therefore, central to cellular metabolism. In addition, NAD⁺ is a substrate for different enzymes, such as sirtuins and poly-ADP ribosylpolymerases (PARPs).⁷ Nicotinamide phosphoribosyltransferase (NAMPT) is the rate-limiting enzyme recovering NAD⁺ from NAM in the NAD⁺ salvage pathway, which is the

predominant pathway by which cells maintain their intracellular NAD⁺ levels.^{8,9} Hence, NAMPT controls intracellular NAD⁺ levels and, consequently, energy metabolism.

Reprogramming of cellular metabolism is one of the hallmarks of cancer.¹⁰ Cancer cells have a higher metabolic demand for ATP and NAD⁺. This is due to the increased levels or activation of several NAD⁺-consuming enzymes in cancer cells compared with normal cells. Examples of such activated enzymes are mono(ADP-ribosyl) transferases (MARTs) and PARPs which transfer the ADP moiety of NAD⁺ to acceptor proteins, resulting in PARylated substrates.¹¹ In response to DNA damage in cancer cells, for example, by DNA damage-

Received: April 11, 2022

Revised: May 17, 2022

Published: June 3, 2022



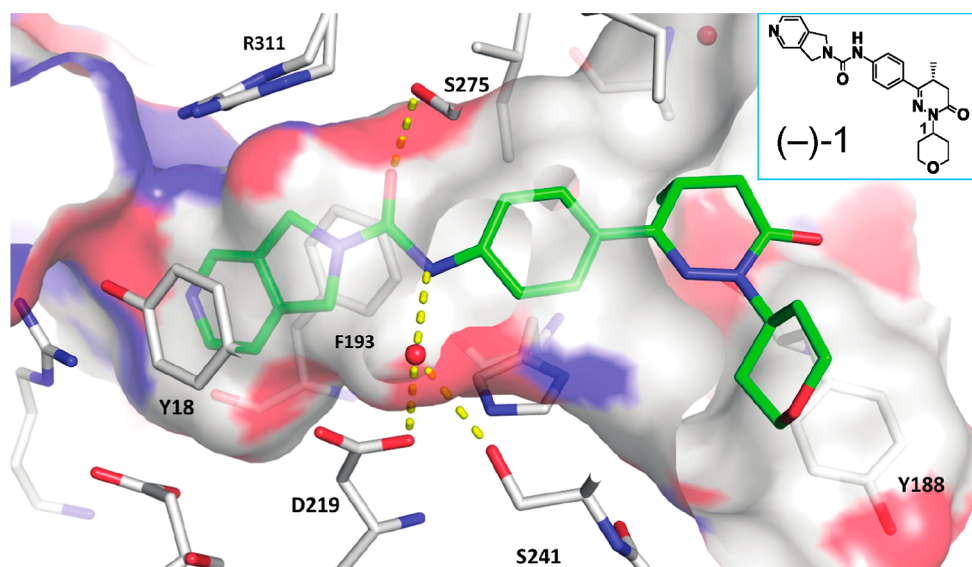


Figure 1. X-ray cocrystal structure of compound (–)-1 in complex with the hNAMPT protein. The structure was determined at 1.86 Å resolution (PDB accession code 7PPE).

inducing chemotherapeutic drugs, PARP1 is recruited and activated and consumes NAD^+ to support the DNA repair. PARP1 expression is increased in several cancers, and in breast cancer also, gene amplification has been reported.^{12,13} Therefore, cancer cells must continuously resynthesize NAD^+ to avoid NAD^+ depletion and ultimately cell death. Indeed, upregulation of NAMPT has been reported in various cancers, such as colorectal, breast, and ovarian cancer.^{9,11}

Several selective small-molecule NAMPT inhibitors (NAMPTis) have been developed and found to potently inhibit NAMPT in cancer cells, resulting in NAD^+ depletion and cytotoxicity.⁸ Moreover, NAMPTis have been shown to decrease tumor growth in preclinical cancer models.¹⁴ Unfortunately, NAMPTis of different chemical classes have shown disappointing results in clinical trials with dose-limiting toxicities, such as thrombocytopenia, retinal, and cardiac toxicities.¹⁴ In order to improve the therapeutic window, NAMPTis have been proposed as payloads for tumor-targeting ADCs. NAMPT inhibition represents a novel mode of action for ADCs.^{15,16} It is not dependent on cell proliferation, which enables targeting of all antigen-positive tumors, regardless of whether tumors consist of resting cells or contain slowly growing or highly proliferative cells.¹⁵

Here, we present the development and preclinical characterization of a new NAMPTi-based payload class applicable for conjugation to diverse antibodies, resulting in ADCs with low aggregation, high potency, and selectivity in antigen-positive cancer models. Pharmacokinetic studies and metabolite profiling were performed to optimize ADC selectivity and to evaluate potential bystander effects. Moreover, we demonstrate—to our knowledge for the first time—the generation of NAMPTi payload metabolites from the NAMPTi-ADCs *in vitro* and *in vivo*.

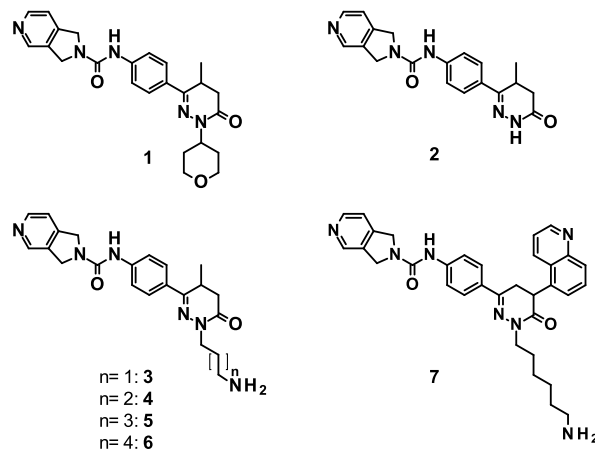
RESULTS

We developed a series of novel and highly potent small-molecule NAMPTis of the pyrrolopyridine class using high-throughput screening combined with structure-based drug design and a set of X-ray structures of the human NAMPT protein (hNAMPT) in complex with different NAMPTis. The

high-resolution structure of compound (–)-1 (Figure 1) highlights the binding mode of this series. Generally, the NAMPT binding pocket features a narrow entrance, where the natural substrate NAM is bound, and a wide funnel opening toward the opposite site. In the NAMPTi series presented, the pyrrolopyridine moiety serves as a NAM mimic. The urea moiety tightly anchors the inhibitor in the pocket through a network of hydrogen bonds, connecting the carbonyl oxygen atom to the Ser275 side chain. On the opposite wall of the pocket, a water molecule mediates hydrogen bonds from the free amino group of the urea to the side chains of Asp219 and Ser241 and to the backbone oxygen atom of Val242. The phenyl ring attached to the urea provides a perfect exit vector into the funnel region when substituted at the para position.

Modeling studies employing both docking and molecular dynamics simulations suggested that, in the funnel region, binding modes are more variable, and their interactions are less stable over time, as compared to the narrower part of the pocket. This estimation of a flatter potential energy landscape in the funnel region was supported by X-ray data demonstrating that, depending on the substitution, even the dihydropyridazinone moiety, attached to position 4 of the aniline, can be accommodated in the NAMPT pocket in various orientations (see compounds 8–11 in Figure S1). While the N1-unsubstituted dihydropyridazinone moiety can participate in hydrogen bonding with Tyr188.O, the N1 position also functions as a suitable attachment point for linkers. Therefore, we investigated several analogues of compound 1 in terms of their effect on NAMPT inhibition. To this end, aminoalkyl chains of different lengths were attached to N1 to enable the connection to a linker *via* the terminal amino group (Table 1).

Compound 1 showed single-digit nanomolar potency ($\text{IC}_{50} = 2.7 \text{ nM}$) toward the hNAMPT protein as determined by the biochemical NAD/NADH-Glo assay (Table 1). The enantiomerically pure compound (–)-1 showed a slightly improved potency with an IC_{50} value of 1.9 nM. Removal of the tetrahydropyran moiety (compound 2) retained the biochemical potency (1.6 nM), while the attachment of an aminopropyl group (compound 3) slightly reduced the

Table 1. Overview of the SAR Analysis: Biochemical and Cellular Potencies of Selected NAMPT Inhibitors^a

compound ^a	amino alkyl carbon chain length	hNAMPT ^b IC ₅₀ (nM)	cellular viability IC ₅₀ (nM) ^c		
			MDA-MB-453 ^d	A549-C4.4a ^e	THP-1 ^f
1	n.a.	2.7	n.d.	n.d.	n.d.
(-)-1	n.a.	1.9	2.7	n.d.	0.34
2	n.a.	1.6	0.65	134	0.47
3	3	2.9	0.78	>300	1.2
4	4	0.8	0.18	63	1.4
5	5	0.8	<0.03	97	0.023
6	6	0.7	<0.03	66	0.0045
7	6	0.2	<0.03	12	<0.003

^aPotencies of selected NAMPTis (^acompounds 1–7 are all racemic apart from (–)-1) were determined in ^bbiochemical and ^ccell-based assays. hNAMPT IC₅₀, IC₅₀ for human recombinant NAMPT determined by NAD/NADH-Glo assay; inhibition of cellular viability IC₅₀, IC₅₀ for NAMPTis determined by CellTiter-Glo assay in MDA-MB-453 breast cancer, A549-C4.4a lung cancer,¹⁷ and THP-1 monocytic leukemia cells. ^dNAMPT mRNA expression: 7200; ^eNAMPT mRNA expression: 66,600; ^fNAMPT mRNA expression: 11,500; NAMPT mRNA expression levels were determined in an Affymetrix microarray (>1100 cancer cell lines) with an average expression level of 50,400; n.a., not applicable, n.d., not determined.

biochemical potency (2.9 nM). Attachment of a longer aminoalkyl chain to the N1 position (aminobutyl, -pentyl, or -hexyl chain in compounds 4, 5, and 6, respectively) resulted in increased potency with IC₅₀ values of 0.7–0.8 nM. Replacement of the methyl-substituted scaffold with a 5-quinolinyl-substituted dihydropyridazinone moiety (compound 7) increased the potency even further, as indicated by an IC₅₀ of 0.2 nM. With a small tilt of the dihydropyridazinone plane compared to compound (–)-1, the quinoline heterocycle finds a favorable orientation in the pocket with an additional H-bond being formed to Lys189 (see Figure S1E). The increased biochemical potency of compounds 4, 5, 6, and 7 translated into markedly improved cellular potency, as demonstrated in three cancer cell lines of different origins (Table 1). Furthermore, the sensitivity of the tested cell lines to NAMPT inhibition inversely correlated with their NAMPT mRNA expression level. In conclusion, the different potencies of NAMPTis reflected the differential sensitivities of the cell lines, of which MDA-MB-453 and THP-1 were highly sensitive and A549-C4.4a was less sensitive to NAMPT inhibition.

Next, compounds 4 and 6 bearing an aminobutyl or aminohexyl chain, respectively, were employed for the construction of ADCs. We used a maleimide for Michael addition reactions with the thiol groups of the antibody that were generated through the reduction of interchain disulfide bonds.¹⁸ For proof-of-concept studies, antibodies targeted against C4.4a (expressed on MDA-MB-453 and A549-C4.4a cells), HER2 (expressed on MDA-MB-453 cells), and B7H3

(expressed on THP-1 cells) were used (for more details, see Supporting Information Methods). To investigate antigen-independent activity of the ADCs, a non-targeted isotype control antibody was used for conjugation.

Altogether, three different effector chemistries (ECs, defined as toxophore + linker) were investigated: EC1 (aminobutyl chain and maleimido-caproyl linker), EC2 (aminohexyl chain and maleimido-caproyl linker), and EC3 (aminobutyl chain and valine-alanine-maleimido-caproyl linker) (see Table 2). EC3 contained a dipeptide (Val-Ala) linker that has been described to be cleaved intracellularly after internalization of the ADC¹⁹ and should, thus, release the NAMPT inhibitor (compound 4 = toxophore) inside the cells. The ADCs evaluated in this study had drug-to-antibody ratios (DARs) of 2.2–7.8 and demonstrated very low aggregation, with a monomer content of ≥95%. The targeted NAMPTi-ADCs demonstrated high cytotoxicity with 1–2 orders of magnitude higher potencies on antigen-expressing cells compared with the potencies observed with the isotype control ADCs. The B7H3-targeting ADC with EC2 effector chemistry, B7H3-EC2, demonstrated the highest potency with an IC₅₀ of 6.9 pM in THP-1 cells. The increased potency of B7H3-EC2 parallels the higher observed potency of the respective NAMPTi compound 6 as compared to B7H3-EC1 (IC₅₀ = 0.19 nM) and the toxophore, compound 4, in THP-1 cells (Table 1). Notably, the non-targeted isotype control ADCs demonstrated cytotoxicity in the highly NAMPTi-sensitive cell line THP-1 with IC₅₀ values of 1.5 nM (EC1), 85 pM (EC2), and 3.4 nM (EC3).

Table 2. *In Vitro* Potencies of NAMPTi-ADCs with Different ECs in MDA-MB-453, A549-C4.4a, and THP-1 Cells

NAMPTi-ADC ^a	R3	Linker	Cytotoxicity, IC ₅₀ (nM)			
			DAR	MDA-MB-453 ^b		
				(C4.4a, HER2)	A549-C4.4a ^c	THP-1 ^d
C4.4a-EC1			3.1	10	240	n.d.
HER2-EC1			2.8	0.076 [#]	n.d.	n.d.
B7H3-EC1			4.2	n.d.	n.d.	0.19
isotype control-EC1			2.6	37	300	1.5
C4.4a-EC2			2.2	0.37	88	n.d.
B7H3-EC2			5.1	n.d.	n.d.	0.0069
isotype control-EC2			3.4	n.d.	91	0.085
C4.4a-EC3			2.8	23	7.1	n.d.
HER2-EC3			3.9	0.061	300	n.d.
B7H3-EC3			4.1	n.d.	n.d.	0.036
isotype control-EC3			3.7	87	300	3.4
C4.4a-EC4			6.4	58	1.3	n.d.
HER2-EC4			2.7	0.036	300	n.d.
HER2-EC4			7.8	<0.0003	>300	n.d.
B7H3-EC4			4.4	n.d.	n.d.	0.0070
isotype control-EC4			3.9	300	300	30
isotype control-EC4			8.0	56	>300	n.d.
C4.4a-EC5			3.6	48	8.4	n.d.
HER2-EC5			4.8	0.043	300	n.d.
B7H3-EC5			5.2	n.d.	n.d.	n.d.
isotype control-EC5			5.3	35	300	n.d.

^aNAMPTi-ADCs were generated by coupling potent NAMPTis discovered in the small-molecule screen (see Table 1) to C4.4a, HER2, B7H3, and non-targeted isotype control antibodies using the following linker types and antibody connection technologies: noncleavable linker and cysteine Michael addition for EC1 and EC2 and cleavable Val-Ala linker and cysteine Michael addition for EC3. All NAMPTi-ADCs were >96% monomers. ^bEndogenous C4.4a, antibodies bound per cell (ABC) ~ 20,000; endogenous HER2, ABC ~ 80,000. ^cTransfected C4.4a, ABC ~ 440,000. ^dEndogenous B7H3, ABC ~ 100,000; EC, effector chemistry; DAR, drug-to-antibody ratio; cytotoxicity IC₅₀, IC₅₀ for NAMPTi-ADCs after a 72 h (# = 96 h) treatment determined by CellTiter-Glo assay (Promega) in MDA-MB-453 breast cancer, A549-C4.4a lung cancer, and THP-1 monocytic leukemia cells, n.d., not determined. Asterisks (*) indicate connection points of R3 and linker structures.

This indicated that ADCs with these ECs may have residual activity and, therefore, may not be optimal, since their potency was not only dependent on the B7H3 antigen.

To better understand the reason for the residual activity of the isotype control ADCs and to further improve the selective,

target-mediated uptake, we next investigated the stability of the payload connection to the antibody and the intracellular fate of the payload by measuring the generation of EC3-ADC metabolites in A549 cells by ultraperformance liquid chromatography coupled to high-resolution mass spectrometry.

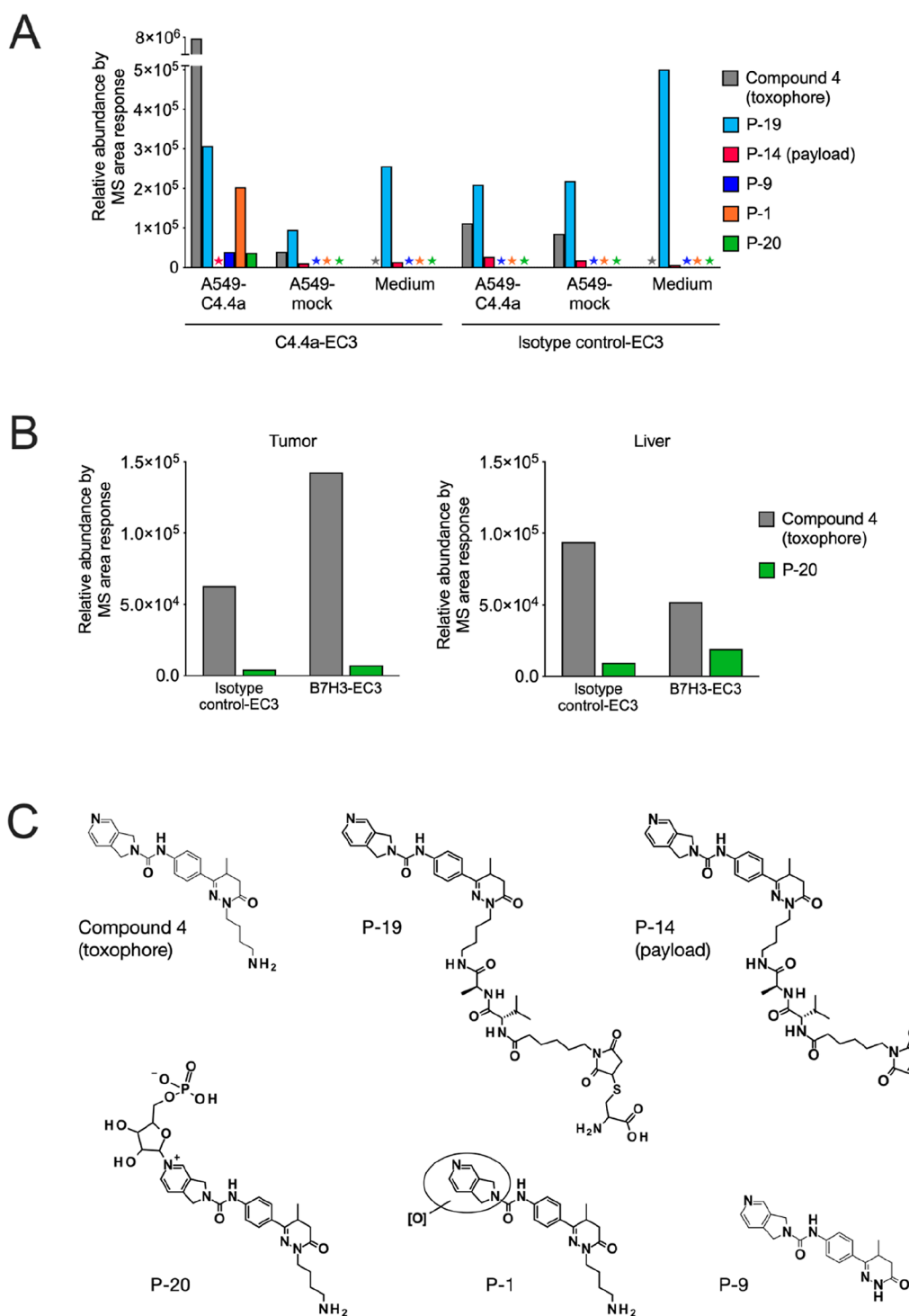


Figure 2. Metabolism of NAMPTi-ADCs with EC3. (A) *In vitro* formation of metabolites in C4.4a-expressing and mock A549 cells after treatment with C4.4a-EC3 or isotype control-EC3 for 24 h, expressed as relative mass spectrometric area response after HPLC-MS analysis. Medium was used as the control. Stars indicate that the specific metabolites were below the limit of detection. (B) *In vivo* formation of the phosphoribosylated metabolite P-20 in tumor and liver of THP-1 tumor-bearing mice after treatment with B7H3-EC3 or isotype control-EC3 [5 mg/kg, Q3/4Dx3, intravenous (i.v.)] for 24 h. (C) Structures of EC3-ADC metabolites. [O] in compound P-1 indicates oxidation of the bicyclic ring.

try. In target antigen-expressing A549-C4.4a cells, marked formation of compound 4 (free toxophore of EC3), minor degradation products P-1 and P-10, and the degradation products P-14 and P-19, both containing linker constituents, was observed (Figure 2, Table S1, and Figure S4). The formation of the phosphoribosylated metabolite P-20 was also detected (Figure 2A,B), confirming our hypothesis that

NAMPT phosphoribosylates the NAM-mimicking NAMPTi-ADC payload, resulting in NAD⁺ depletion and, eventually, cell death. Interestingly, the formation of the Cys metabolite P-19 with an intact linker was observed both in targeted A549-C4.4a and non-targeted A549-mock cells, and even in growth medium-treated and isotype control ADC-treated cells (Figure 2A,C). This suggested payload deconjugation from the

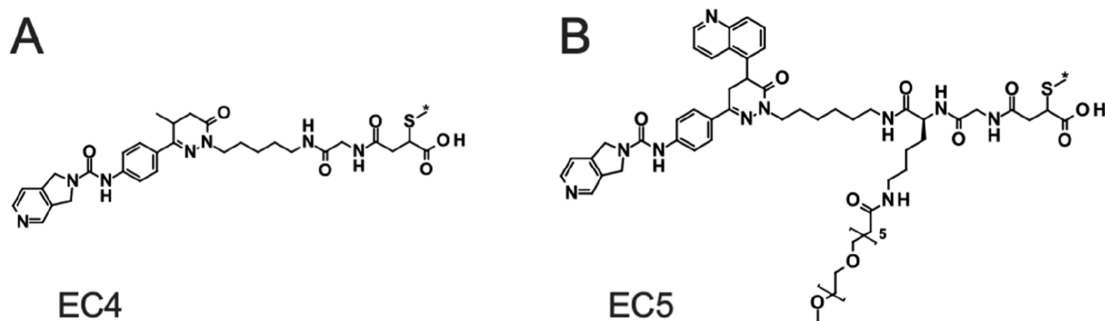


Figure 3. Optimized ECs (A) EC4 and (B) EC5. EC4 was used for the NAMPTi-ADCs that were tested *in vivo*.

Table 3. Permeability, Biochemical Potency, and Cellular Cytotoxicity of the Expected Metabolites of NAMPTi-ADCs with Different ECs

Metabolite	Effector chemistry	P_{app} A-B ^a (nm/s)	P_{app} B-A ^b (nm/s)	hNAMPT ^c IC ₅₀ (nM)	Cytotoxicity, IC ₅₀ (nM) ^d		
					MDA-MB-453	A549-C4.4a	THP-1
	EC1	4.0	4.2	1.5	8.1	>300	1.9
	EC2	1.8	7.0	0.92	0.13	289	0.21
	EC4	7.5	7.8	1.4	129	>300	72
	EC5	0.7	2.7	1.4	>300	>300	63

The apparent permeability P_{app} for both the ^aapical to basolateral (A → B) and the ^bbasolateral to apical (B → A) direction was assessed in a permeability assay with Caco-2 cells. The potency of the metabolites of NAMPTi-ADCs with EC1, EC2, EC4, or EC5 was evaluated using ^cbiochemical and ^dcellular assays. EC, effector chemistry; cytotoxicity IC₅₀, IC₅₀ for NAMPTi-ADCs determined by CellTiter-Glo assay (Promega) in MDA-MB-453 breast cancer, A549-C4.4a lung cancer, and THP-1 monocytic leukemia cells.

antibody, possibly contributing to the observed residual activity of the isotype control ADCs. The formation of the phosphoribosylated derivative P-20 was confirmed by incubation of the free toxophore (compound 4) with recombinant NAMPT, resulting in the formation of the identical derivative P-20 (Figure S3). The phosphoribosylated metabolite P-20 was also detected in liver and tumor samples of THP-1 tumor-bearing mice after treatment with a B7H3-targeting EC3-ADC (Figure 2B and Table S2). This

demonstrates, to our knowledge, for the first time the mode of action and metabolism of NAMPTi-ADCs *in vivo*.

Based on these observations, our strategy to decrease the non-target-mediated cellular activity and to increase the therapeutic window was based on decreasing payload deconjugation from the antibody and decreasing possible metabolite bystander effects. In contrast to a succinimide, a negatively charged succinic amide linkage can prevent the elimination of the cysteine residue or antibody from the payload.²¹ Therefore, an open-chain succinic amide was

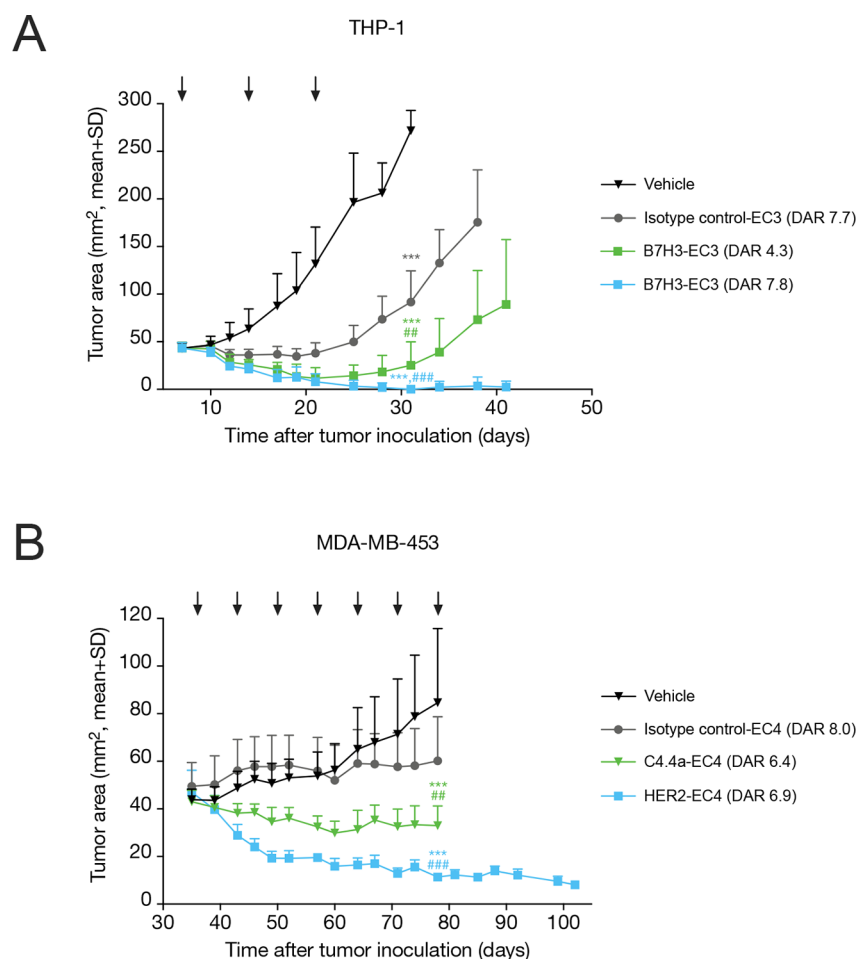


Figure 4. *In vivo* antitumor efficacy of C4.4a-, HER2-, and B7H3-targeted NAMPTi-ADCs. (A) Growth curves of THP-1 tumors in female scid mice ($n = 7$ /group) treated with vehicle, B7H3-EC3 (DAR 4.3 or 7.8), or isotype control-EC3 (5 mg/kg, i.v., Q7Dx3), as indicated by black arrows. (B) Growth curves of MDA-MB-453 tumors in female NOD-scid mice ($n = 7-10$ mice/group) treated with vehicle, C4.4a-EC4, HER2-EC4, or isotype control-EC4 (10 mg/kg, i.v., Q7Dx7), as indicated by black arrows. Statistical analyses were performed using the estimated linear model corrected with Sidak's or Tukey's method. i.v., intravenously, Q7D, every 7 days; ***, $P < 0.001$ vs vehicle; ##, $P < 0.01$; and ###, $P < 0.001$ vs isotype control.

generated at the antibody using a glycine maleimide as the Michael acceptor, followed by basic opening of the resulting succinimide at pH 8.²² This strategy led to the generation of the ECs EC4 and EC5 (Figure 3), based on the NAMPTi compounds 5 (aminopentyl) and 7 (aminohexyl 5-quinolinyl) (Table 1), respectively. To reduce potential aggregation of the ADCs, the increased lipophilicity of the 5-quinolinyl group in EC5 was balanced by the addition of a PEG6 chain in the linker moiety.^{23,24}

EC4- and EC5-ADCs achieved high DARs with a low tendency for aggregation (monomer ratio $\geq 95\%$), high potencies, and very high selectivity in target antigen-expressing cancer cells compared to non-target-expressing cells and to isotype control ADCs (Table 2). EC4-ADCs demonstrated a very beneficial technical profile allowing the conjugation of up to eight payloads per antibody without notable aggregation. B7H3-EC4 showed very high potency in THP-1 cells with an IC_{50} value of 7 pM. For HER2-EC4, the observed IC_{50} value in MDA-MB-453 cells was even below the assay threshold level (0.3 pM). In contrast, the corresponding isotype control ADCs demonstrated IC_{50} values of 30 and 56 nM in THP-1 and MDA-MB-453 cells, respectively. This resulted in $Q_{IC_{50}}$ (= IC_{50} of mock cells/ IC_{50} of antigen-expressing cells) values of

>4000 in the B7H3/THP-1 setting and >150,000 in the HER2/MDA-MB-453 setting, suggesting that a wide therapeutic window could be achieved in the *in vivo* experiments. Furthermore, a 24–48 h treatment with EC4-ADCs resulted in marked NAD^+ depletion in target antigen-expressing cells compared to non-target-expressing or isotype control ADC-treated cells (Table S3). For EC5-ADCs, the highest potency was observed for HER2-EC5 with an IC_{50} of 43 pM in MDA-MB-453 cells, whereas the corresponding isotype control ADC had an IC_{50} of 35 nM, indicating more than 800-fold selectivity for HER2-EC5 (Table 2).

To further investigate potential bystander effects of the different NAMPTi-based ECs, we evaluated the permeability, biochemical potency, and *in vitro* cytotoxicity of the assumed metabolites of EC1, EC2, EC4, and EC5 (Table 3). High biochemical potencies toward hNAMPT with nanomolar IC_{50} values were observed for all metabolites. The permeability of all metabolites was low in the CaCo-2 assay ($P_{app} A-B$ and $P_{app} B-A < 10$ nm/s), indicating a low bystander effect. Nonetheless, in selected cancer cell lines, pronounced cytotoxicity was observed for the metabolites of NAMPTi-ADCs with maleimide-conjugated payloads (EC1 and EC2). In contrast, the metabolites of NAMPTi-ADCs with the

optimized ECs EC4 and EC5 showed very low cytotoxicity, indicating that the low permeability observed in the CaCo-2 assay may not be predictive of cytotoxicity.

Finally, we evaluated the *in vivo* antitumor efficacy of optimized NAMPTi-ADCs in target antigen-expressing xenograft mouse models. B7H3-targeted NAMPTi-ADCs with EC3 showed high *in vivo* antitumor efficacy in the THP-1 acute myeloid leukemia (AML) xenograft model in scid mice (Figure 4A). Treatment with the high-DAR B7H3-EC3 (DAR 7.8; 5 mg/kg, *i.v.*, Q7Dx3) effectively inhibited tumor growth with a T/C (treatment/control) ratio of 0.00 ($p < 0.001$ vs vehicle) and resulted in complete responses in 6/7 mice and partial responses (PRs) in 1/7 mice. In contrast, treatment with the low-DAR B7H3-EC3 (DAR 4.3; 5 mg/kg, *i.v.*, Q7Dx3) resulted in a T/C of 0.09 ($p < 0.001$ vs vehicle) and PRs in 2/7 and progressive diseases (PDs) in 5/7 mice. A higher selectivity of the B7H3-EC3 ADCs compared with the non-targeted isotype control-EC3 was observed in the tumor regrowth phase after the treatment had been stopped (day 21). These results are in line with the results obtained in THP-1 cells *in vitro* (Table S4). All treatments were well tolerated with a maximum body weight loss of less than 10% (Figure S2A).

C4.4a- and HER2-targeted NAMPTi-ADCs with EC4 showed high *in vivo* antitumor efficacy in the MDA-MB-453 breast cancer xenograft model in NOD-scid mice (Figure 4B). C4.4a-EC4 (10 mg/kg, *i.v.*, Q7Dx7) inhibited tumor growth with a T/C of 0.39 ($p < 0.001$ vs vehicle) and resulted in PRs in 3/8 mice and stable diseases in 5/8 mice. Treatment with HER2-EC4 (10 mg/kg, *i.v.*, Q7Dx7) resulted in marked tumor growth inhibition (T/C = 0.13, $p < 0.001$ vs vehicle) with 7/7 PRs in mice. After cessation of the treatment, no tumor regrowth was observed in this group. The efficacy of the targeted EC4-ADCs was selective as compared with the non-targeted isotype control-EC4. All treatments were tolerated with acceptable body weight loss (10–18%) (Figure S2B).

DISCUSSION

Although there is at present a thorough understanding of the targeting mechanism and mechanism of action of NAMPTi-ADCs,^{16,25} previous approaches have shown that there is still considerable room for improvement in generating highly selective, potent, and stable NAMPTi-ADCs with low aggregation propensities and potential for effective treatment of hematological and solid cancers. Here, we identify two promising NAMPTi-ADCs with the optimized ECs EC4 and EC5 that overcome previous challenges of NAMPTi-based ADCs.

Earlier studies have introduced NAMPTi-ADCs with potent *in vitro* and *in vivo* efficacies, but there have been challenges related to selectivity and toxicity. The NAMPTi-ADC designed by Karpov *et al.*, for example, showed strong aggregation and only moderate selectivity,²⁵ while the NAMPTi-ADCs designed by Neumann *et al.* employed a self-immolating glucuronide-carbamate linker strategy to allow for toxophore liberation in lysosomes, possibly posing a risk to patients due to liberated toxophores entering nontumor cells.^{15,16} Our approach to avoid these issues was to use a conjugation strategy that would result in ADCs with low aggregation, high potency, and selectivity. Furthermore, we wanted to follow a conjugation strategy, resulting in the formation of weakly permeable NAMPTi payload metabolites in tumor cells. This would reduce the impact of liberated payload metabolites on surrounding non-targeted, healthy cells and thus result in

NAMPTi-ADCs with a better safety profile. Therefore, we investigated the stability of the payload connection to the antibody and the intracellular fate of the payload by identifying generated NAMPTi-ADC metabolites. This led to the discovery of phosphoribosylated NAMPTi payload metabolites *in vitro* and *in vivo* and increased our understanding on how to improve linker stability and reduce the permeability of NAMPTi payload metabolites.

The potency of the developed NAMPTis was demonstrated to be dependent on the aminoalkyl chain length attached to the N1 of the dihydropyridazinone in biochemical and cellular assays. This showed that increasing the aminoalkyl chain length led to increased potency. Compound 7, which had a 5-quinolinyl substituent, showed an even further increased biochemical potency. This may reflect the modified binding mode of this compound. The increased potency was also reflected in *in vitro* experiments with different cancer cell lines, where we observed that high sensitivity toward NAMPT inhibition inversely correlated with NAMPT mRNA levels and translated into markedly improved cellular potency. This is in line with the results by Xiao *et al.* who have reported that NAMPT mRNA and protein levels inversely correlate with sensitivity to NAMPTis and that patient stratification based on NAMPT expression could provide an approach to enhance the therapeutic effectiveness of NAMPTis.²⁶

Toxophore compounds 4 (with an aminobutyl chain) and compound 6 (with an aminoethyl chain) were then employed in the construction of ADCs, as they showed high potencies in biochemical and cellular assays and had a suitable linker attachment point *via* the terminal amino group of the aminoalkyl chain. The resulting ADCs showed very low aggregation and a good technical profile with DARs of 2.2–7.8. The comparatively low DARs observed for the C4.4a-targeted ADCs can be explained by the fact that the higher loaded conjugates could have an increased aggregation tendency, and the formed aggregates are removed in the purification step of the ADC preparation. The ADCs also showed antigen-dependent targeting and internalization, as evidenced by their high potencies in antigen-expressing MDA-MB-453 (C4.4a- and HER2-ADCs), A549-C4.4a (C4.4a-ADC), and THP-1 (B7H3-ADC) cells. The corresponding isotype control ADCs showed only residual activity. EC3, bearing a cleavable Val-Ala linker, showed increased potency compared with the noncleavable maleido-caproyl linker-bearing EC1 in A549-C4.4a cells (C4.4a-targeted ADCs) and THP-1 cells (B7H3-targeted ADCs).

Unspecific activity of ADCs, that is, other than target-mediated cellular ADC uptake, is a major concern when treating patients. ADC metabolites can also affect non-target-expressing, healthy tissues and thereby decrease their therapeutic window. Although the residual activity observed with our non-targeted isotype control ADCs was approximately 10-fold lower compared to the targeted NAMPTi-ADCs, we sought to deepen our understanding of the underlying biochemical and cellular mechanisms of ADC metabolism by analyzing the formation of payload metabolites *in vitro* and *in vivo*. These studies revealed *in vitro* the formation of toxophore compound 4 in A549-C4.4a cells as well as—to our knowledge for the first time for a NAMPTi-ADC—*in vivo* the formation of the corresponding phosphoribosylated metabolite P-20 in the THP-1 xenograft model after treatment with B7H3-EC3. These findings support the mode of action of NAMPT inhibition, where the phosphoribosyla-

tion of a NAMPTi-ADC metabolite—instead of the natural substrate NAM—results in decreased NAD^+ levels and further in NAD^+ depletion and cell death.^{8,9} In addition to the formation of toxophore compound 4 and P-20, the formation of the degradation products P-14 and P-19, both containing linker constituents, was observed.

To further decrease the non-target-mediated cellular activity of the NAMPTi-ADCs and to increase their therapeutic window, a strategy to decrease payload deconjugation and subsequent possible metabolite bystander effects was adopted. The formation of toxophore compound 4 could be explained by the intracellular cleavage of the Val-Ala peptide linker in lysosomes. The formation of the free payload P-14 and the cysteine derivative P-19, in turn, could be explained by a retro-Michael reaction generating a free maleimide at the payload P-14 and a Cys-SH at the antibody, followed by a reaction of the maleimide P-14 with cysteine either from the cytosol or from the medium, resulting in the formation of metabolite P-19. In order to stabilize the conjugation of the payload to the antibody, we employed a connection strategy that generated a negatively charged succinic amide, thereby hindering a retro-Michael reaction. Using this connection strategy and a noncleavable linker, we developed ECs EC4 and EC5 that were based on NAMPTi compound 5 and the highly potent 5-quinolinyl analogue compound 7. The resulting EC4- and EC5-ADCs showed high potency in target antigen-expressing cells but only very low potency in non-target-expressing cells. These ADCs also showed good specificity compared to the corresponding isotype control ADCs and induced NAD^+ depletion in cell-based assays. Furthermore, we were able to prepare EC4- and EC5-ADCs with high DARs (up to 8 payloads per antibody) without increasing their aggregation tendency. This was the result of the increased hydrophilicity of not only the anionic succinic amide linkage but also the PEG-6 side chain employed in EC5, designed to balance the lipophilicity of the 5-quinolinyl substituent.

As the aim was to reduce the systemic toxicity caused by unspecific uptake of the generated ADC metabolites into non-target antigen-expressing cells, we evaluated the cellular activity of the expected payload metabolites formed within tumor cells upon treatment with EC1-, EC2-, EC4-, or EC5-ADCs. When tumor cells die, the formed payload metabolites are released into the tumor microenvironment, and thus, their cytotoxic effects on the surrounding tissue depend on their permeability.^{27,28} In our *in vitro* cytotoxicity studies, EC1 and EC2 metabolites showed high cytotoxic potency toward the different cancer cell lines employed in this study. In contrast, the cytotoxic potency of EC4 and EC5 metabolites was very low despite their high biochemical potency. This indicated that the cellular permeability of these metabolites was even further reduced compared to that of EC1 and EC2 metabolites. The reduced permeability leading to the low cytotoxic potency of EC4 and EC5 could be explained by the high polarity of the cysteine-substituted succinic amide moiety related to the additional carboxylic acid groups and the PEG6 side chain in EC4 and EC5. These findings supported our strategy to restrict the ADC activity to target antigen-expressing cells by reducing possible bystander effects of the metabolites.

Because the developed NAMPTi-ADCs showed high *in vitro* potency and selectivity and induced NAD^+ depletion in target antigen-expressing cancer cells, we tested them further in *in vivo* tumor models. The HER2-, C4.4a-, and B7H3-targeted NAMPTi-ADCs exhibited potent antitumor activity with

acceptable tolerability, as demonstrated in the THP-1 AML and MDA-MB-435 breast cancer xenograft models. In the THP-1 model, treatment with B7H3-targeted EC3-ADCs almost completely eradicated all tumors, and notably, no tumor regrowth was observed after cessation of treatment. Accordingly, in the MDA-MB-435 model, marked tumor growth inhibition was observed upon treatment with HER2- and C4.4a-targeted EC4-ADCs. Treatment with HER2-EC4 was even more efficacious than treatment with C4.4a-EC4, demonstrated by T/C values of 0.13 and 0.39, respectively. In MDA-MB-453 cells, the expression level of HER2 receptors was approximately fourfold compared with C4.4a receptors, which could in part explain the enhanced antitumor efficacy of HER2-EC4. Moreover, the antibody used in C4.4a-EC4 is cross-reactive with the mouse C4.4a antigen, whereas the antibody used in HER2-EC4 is not cross-reactive. This could also contribute to the observed differential effects of C4.4a-EC4 and HER2-EC4 on tumor growth and body weight in the MDA-MB-435 xenograft model. Overall, the EC4-ADCs showed high selectivity compared with the corresponding isotype control ADC, which had no apparent *in vivo* activity, highlighting the good performance of the optimized ECs. Importantly, in this study, we demonstrated for the first time the generation of NAMPTi payload metabolites both *in vitro* and *in vivo*, shedding more light on the mode of action of NAMPTi-ADCs. Taken together, these findings provide a holistic understanding of the fate of ADCs starting from their cellular uptake down to the intracellular interaction of the ADC metabolites with their target, the NAMPT enzyme. In conclusion, our study suggests that NAMPTis represent an attractive new payload class designed for use in ADCs for the treatment of solid and hematological tumors.

EXPERIMENTAL PROCEDURES

Synthesis instructions for compounds 1–7, all ECs and their metabolites, and the ADCs and detailed descriptions of the methods are provided in the [Supporting Information](#).

Analytical Characterization of ADCs. Drug-to-antibody ratio determination, purity assessment, and determination of the concentration of the ADCs were performed as described in [Supporting Information Methods](#).

Cell Lines. Caco-2 human colorectal adenocarcinoma and MDA-MB-453 human breast cancer cell lines were obtained from DSMZ (German Collection of Microorganisms and Cell Cultures). A549 human lung cancer and THP-1 human monocytic leukemia cell lines were obtained from ATCC (American Type Culture Collection). All cell lines were cultured according to the provider's instructions. The A549-C4.a cell line, transfected to overexpress the C4.4a antigen, was generated as described by Willuda *et al.*¹⁷ All cell lines were obtained during 2002–2016 and authenticated using short tandem repeat DNA fingerprinting at DSMZ before the experiments and subjected frequently to mycoplasma testing.

In Vitro Assays. The inhibitory activity of each ADC on the hNAMPT protein (hNAMPT IC₅₀) was determined using a biochemical NAMPT inhibition assay. The *in vitro* potencies of NAMPTis and NAMPTi-ADCs were determined in human MDA-MB-453 breast cancer, A549-C4.4a lung cancer, and THP-1 monocytic leukemia cells using the CellTiter-Glo cell viability assay (Promega, Madison, WI, USA). The cell permeability of the NAMPTi payload metabolites was investigated with an *in vitro* flux assay in Caco-2 cells. NAMPTi payload metabolites were identified using high-

performance liquid chromatography/mass spectrometry (HPLC–MS) analysis. Detailed descriptions for all assays are provided in Supporting Information Methods.

In Vivo Studies. All animal studies were conducted in accordance with the German Animal Welfare Law and approved by Berlin authorities (Landesamt für Gesundheit und Soziales (LAGeSo), Berlin; Anzeigen-Code A0378/12). The *in vivo* antitumor efficacy and tolerability of the selected NAMPTi-ADCs were evaluated in the cell line-derived THP-1 human AML and MDA-MB-453 human breast cancer xenograft models. Detailed method descriptions are provided in the Supporting Information Briefly, THP-1 tumor-bearing female scid (scid/scid) mice ($n = 7$ mice/group) were treated with i.v. injections of vehicle (5 mL/kg), B7H3-EC3 (DAR 4.3 or 7.8), or isotype control-EC3 (TPP-754, DAR 7.7) at 5 mg/kg once weekly (Q7D) for 3 weeks (last dosing on day 21). The study was terminated on day 34 after tumor cell inoculation. MDA-MB-453 tumor-bearing female NOD-scid mice ($n = 7–10$ mice/group) were treated with i.v. injections of vehicle, C4.4a-EC4 (first DAR 7.1 and then DAR 6.4 from day 64 onward), HER2-EC4 (DAR 7.8), or isotype control-EC4 (TPP-754 and DAR 8.0) at 10 mg/kg (Q7D) for 7 weeks. The study was terminated on day 102 after tumor cell inoculation.

For assessing the *in vivo* formation of the phosphoribosylated metabolite P-20, THP-1 tumor-bearing mice of the vehicle-treated group in the antitumor efficacy study were allocated to a final single-dose treatment on day 30 after tumor cell inoculation. The mice were treated with an i.v. injection of B7H3-EC3 (DAR 4.3; $n = 3$) or with isotype control-EC3 (TPP-754, DAR 8.3; $n = 2$) at 10 mg/kg, the animals were euthanized 24 h postinjection, and plasma, tumor, and liver samples were collected.

Statistical Analyses. All analyses were performed using the statistical programming language R [R version 3.6.3 (2020-02-29)]. Validity of the model assumptions was checked for the fitted statistical model. The analyses were performed using linear models estimated with generalized least squares with a separate variance term for each group. Pairwise comparisons were performed using the estimated linear model and corrected for familywise error rate using Sidak's or Tukey's method where appropriate.

■ ASSOCIATED CONTENT

SI Supporting Information

The Supporting Information is available free of charge at <https://pubs.acs.org/doi/10.1021/acs.bioconjchem.2c00178>.

Crystal structures of hNAMPT in complex with four different NAMPTis, body weight change in THP-1 and MDA-MB-453 xenograft models, structure elucidation of metabolites of NAMPTi-ADCs, identification of NAMPTi-ADC metabolites in A549-C4.4 cancer cells, SEC-UV analysis of TPP-1015 ADC with EC4, mass spectrum of a TPP-1015 ADC with EC4 after reduction with DTT, *in vitro* formation of NAMPTi metabolites and their proposed mode of formation in target antigen-expressing A549-C4.4a cells, *in vivo* formation of NAMPTi-ADC payload metabolites and their proposed mode of formation in target antigen-expressing THP-1 tumor-bearing mice, NAD⁺ depletion of C4.4a- and HER2-targeted NAMPTi-ADCs with effector chemistry EC4 in MDA-MB-453, A549-C4.4a, and A549-mock cells, *in*

vitro potency of B7H3-targeted and isotype control NAMPTi-ADCs with effector chemistry EC3 in THP-1 cells, employed antibody and reagent amounts and analytical data of the generated EC1-ADCs, EC2-ADCs, EC3-ADCs, EC4-ADCs, and EC5-ADCs, absorption coefficients for the antibodies and drugs, summary of analytical data of all ADCs, NAMPT crystallographic data collection and refinement statistics, assay conditions for cell lines in the CTG cell proliferation assay, assay kits and antibodies used in flow cytometry analyses, synthesis of NAMPTis: compounds 1–7, synthesis of ADC precursors, synthesis of metabolites, synthesis of ADCs, analytical characterization of ADCs, structural biology, *in vitro* assays, metabolite identification methods, *in vivo* studies, accession codes, determination of purity, and ¹H NMR spectra of key compounds (PDF)

■ AUTHOR INFORMATION

Corresponding Author

Niels Böhnke – Bayer AG, Pharmaceuticals, Berlin 13353, Germany; orcid.org/0000-0001-7154-4986; Email: niels.boehnke@bayer.com

Authors

Markus Berger – Bayer AG, Pharmaceuticals, Berlin 13353, Germany; orcid.org/0000-0001-6676-6090

Nils Griebenow – Bayer AG, Pharmaceuticals, Wuppertal 42113, Germany; Present Address: Elanco Animal Health, Lead Discovery & Chemistry, Discovery Research, Alfred-Nobel-Straße 50, 40789 Monheim, Germany

Antje Rottmann – Bayer AG, Pharmaceuticals, Berlin 13353, Germany

Michael Erkelenz – Bayer AG, Pharmaceuticals, Berlin 13353, Germany; Present Address: Nuvisan ICB GmbH, Müllerstraße 178, 13342 Berlin, Germany.

Stefanie Hammer – Bayer AG, Pharmaceuticals, Berlin 13353, Germany

Sandra Berndt – Bayer AG, Pharmaceuticals, Berlin 13353, Germany

Judith Günther – Bayer AG, Pharmaceuticals, Berlin 13353, Germany; orcid.org/0000-0001-5794-8984

Antje M. Wengner – Bayer AG, Pharmaceuticals, Berlin 13353, Germany

Beatrix Stelte-Ludwig – Bayer AG, Pharmaceuticals, Wuppertal 42113, Germany; Present Address: Vincerox Pharma GmbH, Alfred-Nobel-Straße 10, 40789 Monheim, Germany.

Christoph Mahlert – Bayer AG, Pharmaceuticals, Wuppertal 42113, Germany; orcid.org/0000-0003-3272-7856

Simone Greven – Bayer AG, Pharmaceuticals, Wuppertal 42113, Germany

Lisa Dietz – Bayer AG, Pharmaceuticals, Wuppertal 42113, Germany

Hannah Jörißen – Bayer AG, Pharmaceuticals, Wuppertal 42113, Germany

Naomi Barak – Bayer AG, Pharmaceuticals, Berlin 13353, Germany; orcid.org/0000-0002-8166-9616

Ulf Bömer – Bayer AG, Pharmaceuticals, Berlin 13353, Germany; Present Address: Nuvisan ICB GmbH, Müllerstraße 178, 13342 Berlin, Germany.

Roman C. Hillig – Bayer AG, Pharmaceuticals, Berlin 13353, Germany; Present Address: Nuvisan ICB GmbH, Müllerstraße 178, 13342 Berlin, Germany.

Uwe Eberspaecher – Bayer AG, Pharmaceuticals, Berlin 13353, Germany

Jörg Weiske – Bayer AG, Pharmaceuticals, Berlin 13353, Germany; Present Address: Nuvisan ICB GmbH, Müllerstraße 178, 13342 Berlin, Germany.

Anja Giese – Bayer AG, Pharmaceuticals, Berlin 13353, Germany

Dominik Mumberg – Bayer AG, Pharmaceuticals, Berlin 13353, Germany; Present Address: Adcendo ApS, Ole Maaloes Vej 3, 2200 Copenhagen N, Denmark.

Carl Friedrich Nising – Bayer AG, Pharmaceuticals, Berlin 13353, Germany; orcid.org/0000-0002-9931-7096

Hilmar Weinmann – Bayer AG, Pharmaceuticals, Berlin 13353, Germany; Present Address: Janssen Pharmaceutica N.V., Turnhoutseweg 30, 2340 Beerse, Belgium.

Anette Sommer – Bayer AG, Pharmaceuticals, Berlin 13353, Germany; Present Address: Pfizer Worldwide Research, Development and Medical, Linkstraße 10, 10785 Berlin, Germany.; orcid.org/0000-0002-1576-3110

Complete contact information is available at:

<https://pubs.acs.org/10.1021/acs.bioconjchem.2c00178>

Notes

The authors declare the following competing financial interest(s): All authors are current or former employees of Bayer AG. NB, MB, ME, SH, SB, JG, CM, HJ, NBa, UB, RCH, JW, CFN, HW, and AS are stockholders of Bayer AG. All authors (except RCH, UE, JW, DM, CFN, and HW) hold patents connected to this work (WO2019/149637A1, WO2021/013693A1).

ACKNOWLEDGMENTS

We thank Birgit Albrecht, Vivian Bell, Susanne Bendix, Thorsten Boldt, Henryk Bubik, Sebastian Deitz, Norman Dittmar, Charlene Döring, Lisa Ehresmann, Chris Fiedler, Nils Guthof, Achim Korthals, Christopher Kossmann, Marion Kuzora, Dennis Kwiatkowski, Jessica Möllmann, Stephanie Osterberg, Marion Pletsch, Marina Pöhlmann, Maria Ritter, Sabine Schnabel, Stefan Stargard, Carsten Sternberger, Rukiye Tamm, and Sandra Zickelbein for technical assistance. We thank Rudolf Beier for database analyses of cell lines. We thank Ursula Mönning for the Caco-2 assay measurements. We thank the staff at beamline BL14.1 at Helmholtz-Zentrum Berlin (a member of the Helmholtz Association) for access to synchrotron radiation and support during data collection and the staff at moloX GmbH for data collection services. We thank Bertolt Kreft and Lars Linden for fruitful discussions. Anna Huhtinen and Sanna-Maria Käkönen at Aurexel Life Sciences Ltd. (www.aurexel.com) are acknowledged for editorial support funded by Bayer AG.

REFERENCES

- (1) Baah, S.; Laws, M.; Rahman, K. M. Antibody-Drug Conjugates-A Tutorial Review. *Molecules* **2021**, *26*, 2943.
- (2) Chau, C. H.; Steeg, P. S.; Figg, W. D. Antibody-drug conjugates for cancer. *Lancet* **2019**, *394*, 793–804.
- (3) Hafeez, U.; Parakh, S.; Gan, H. K.; Scott, A. M. Antibody-Drug Conjugates for Cancer Therapy. *Molecules* **2020**, *25*, 4764.
- (4) Jiang, J.; Li, S.; Shan, X.; Wang, L.; Ma, J.; Huang, M.; Dong, L.; Chen, F. Preclinical safety profile of disitamab vedotina novel anti-HER2 antibody conjugated with MMAE. *Toxicol. Lett.* **2020**, *324*, 30–37.
- (5) Tong, J. T. W.; Harris, P. W. R.; Brimble, M. A.; Kavianinia, I. An Insight into FDA Approved Antibody-Drug Conjugates for Cancer Therapy. *Molecules* **2021**, *26*, 5847.
- (6) Joubert, N.; Beck, A.; Dumontet, C.; Denevault-Sabourin, C. Antibody-Drug Conjugates: The Last Decade. *Pharmaceuticals* **2020**, *13*, 245.
- (7) Navas, L. E.; Carnero, A. NAD(+) metabolism, stemness, the immune response, and cancer. *Signal Transduction Targeted Ther.* **2021**, *6*, 2.
- (8) Galli, U.; Colombo, G.; Travelli, C.; Tron, G. C.; Genazzani, A. A.; Grolla, A. A. Recent Advances in NAMPT Inhibitors: A Novel Immunotherapeutic Strategy. *Front. Pharmacol.* **2020**, *11*, 656.
- (9) Garten, A.; Schuster, S.; Penke, M.; Gorski, T.; de Giorgis, T.; Kiess, W. Physiological and pathophysiological roles of NAMPT and NAD metabolism. *Nat. Rev. Endocrinol.* **2015**, *11*, 535–546.
- (10) Hanahan, D.; Weinberg, R. A. Hallmarks of cancer: the next generation. *Cell* **2011**, *144*, 646–674.
- (11) Sampath, D.; Zabka, T. S.; Misner, D. L.; O'Brien, T.; Dragovich, P. S. Inhibition of nicotinamide phosphoribosyltransferase (NAMPT) as a therapeutic strategy in cancer. *Pharmacol. Ther.* **2015**, *151*, 16–31.
- (12) Ossovskaya, V.; Koo, I. C.; Kaldjian, E. P.; Alvares, C.; Sherman, B. M. Upregulation of Poly (ADP-Ribose) Polymerase-1 (PARP1) in Triple-Negative Breast Cancer and Other Primary Human Tumor Types. *Genes Cancer* **2010**, *1*, 812–821 From NLM PubMed-not-MEDLINE.
- (13) Zhang, X.; Wang, Y.; A, G.; Qu, C.; Chen, J. Pan-Cancer Analysis of PARP1 Alterations as Biomarkers in the Prediction of Immunotherapeutic Effects and the Association of Its Expression Levels and Immunotherapy Signatures. *Front. Immunol.* **2021**, *12*, 721030 From NLM Medline.
- (14) Ghanem, M. S.; Monacelli, F.; Nencioni, A. Advances in NAD-Lowering Agents for Cancer Treatment. *Nutrients* **2021**, *13*, 1665.
- (15) Hasmann, M.; Schemainda, I. FK866, a highly specific noncompetitive inhibitor of nicotinamide phosphoribosyltransferase, represents a novel mechanism for induction of tumor cell apoptosis. *Cancer Res.* **2003**, *63*, 7436–7442.
- (16) Neumann, C. S.; Olivas, K. C.; Anderson, M. E.; Cochran, J. H.; Jin, S.; Li, F.; Loftus, L. V.; Meyer, D. W.; Neale, J.; Nix, J. C.; et al. Targeted Delivery of Cytotoxic NAMPT Inhibitors Using Antibody-Drug Conjugates. *Mol. Cancer Ther.* **2018**, *17*, 2633–2642.
- (17) Willuda, J.; Linden, L.; Lerchen, H.-G.; Kopitz, C.; Stelte-Ludwig, B.; Pena, C.; Lange, C.; Golfer, S.; Kneip, C.; Carrigan, P. E.; et al. Preclinical Antitumor Efficacy of BAY 1129980-a Novel Auristatin-Based Anti-C4.4A (LYPD3) Antibody-Drug Conjugate for the Treatment of Non-Small Cell Lung Cancer. *Mol. Cancer Ther.* **2017**, *16*, 893–904.
- (18) Doronina, S. O.; Toki, B. E.; Torgov, M. Y.; Mendelsohn, B. A.; Cerveny, C. G.; Chace, D. F.; DeBlanc, R. L.; Gearing, R. P.; Bovee, T. D.; Siegall, C. B.; et al. Development of potent monoclonal antibody auristatin conjugates for cancer therapy. *Nat. Biotechnol.* **2003**, *21*, 778–784.
- (19) Dal Corso, A.; Cazzamalli, S.; Gébleux, R.; Mattarella, M.; Neri, D. Protease-Cleavable Linkers Modulate the Anticancer Activity of Noninternalizing Antibody-Drug Conjugates. *Bioconjugate Chem.* **2017**, *28*, 1826–1833.
- (20) Karlsson, J.; Hagemann, U. B.; Schatz, C.; Grant, D.; Kristian, A.; Ellingsen, C.; Mihaylova, D.; Geraudie, S.; Indrevoll, B.; Wirtzner, U.; et al. Abstract 5859: HER2-targeted thorium-227 conjugate (HER2-TTC): Efficacy in preclinical models of trastuzumab and T-DM1 resistance. *Cancer Res.* **2017**, *77*, 5859.
- (21) Lerchen, H. G.; Wittrock, S.; Stelte-Ludwig, B.; Sommer, A.; Berndt, S.; Griebenow, N.; Rebstock, A. S.; Johannes, S.; Cancho-Grande, Y.; Mahlert, C.; et al. Antibody-Drug Conjugates with Pyrrole-Based KSP Inhibitors as the Payload Class. *Angew. Chem., Int. Ed. Engl.* **2018**, *57*, 15243–15247.

(22) Tumej, L. N.; Charati, M.; He, T.; Sousa, E.; Ma, D.; Han, X.; Clark, T.; Casavant, J.; Loganzo, F.; Barletta, F.; et al. Mild method for succinimide hydrolysis on ADCs: impact on ADC potency, stability, exposure, and efficacy. *Bioconjugate Chem.* **2014**, *25*, 1871–1880.

(23) Giese, M. W.; Woodman, R. H.; Hermanson, G. T.; Davis, P. D. *Chemical Linkers in Antibody-Drug Conjugates (ADCs)*; The Royal Society of Chemistry, 2022; pp 286–376.

(24) Zhao, R. Y.; Wilhelm, S. D.; Audette, C.; Jones, G.; Leece, B. A.; Lazar, A. C.; Goldmacher, V. S.; Singh, R.; Kovtun, Y.; Widdison, W. C.; et al. Synthesis and evaluation of hydrophilic linkers for antibody-maytansinoid conjugates. *J. Med. Chem.* **2011**, *54*, 3606–3623 From NLM Medline.

(25) Karpov, A. S.; Abrams, T.; Clark, S.; Raikar, A.; D'Alessio, J. A.; Dillon, M. P.; Gesner, T. G.; Jones, D.; Lacaud, M.; Mallet, W.; et al. Nicotinamide Phosphoribosyltransferase Inhibitor as a Novel Payload for Antibody-Drug Conjugates. *ACS Med. Chem. Lett.* **2018**, *9*, 838–842.

(26) Xiao, Y.; Elkins, K.; Durieux, J. K.; Lee, L.; Oeh, J.; Yang, L. X.; Liang, X.; DelNagro, C.; Tremayne, J.; Kwong, M.; et al. Dependence of tumor cell lines and patient-derived tumors on the NAD salvage pathway renders them sensitive to NAMPT inhibition with GNE-618. *Neoplasia* **2013**, *15*, 1151–IN23.

(27) Drago, J. Z.; Modi, S.; Chandarlapaty, S. Unlocking the potential of antibody-drug conjugates for cancer therapy. *Nat. Rev. Clin. Oncol.* **2021**, *18*, 327–344.

(28) Li, F.; Emmerton, K. K.; Jonas, M.; Zhang, X.; Miyamoto, J. B.; Setter, J. R.; Nicholas, N. D.; Okeley, N. M.; Lyon, R. P.; Benjamin, D. R.; et al. Intracellular Released Payload Influences Potency and Bystander-Killing Effects of Antibody-Drug Conjugates in Preclinical Models. *Cancer Res.* **2016**, *76*, 2710–2719.